Front. Chem. Sci. Eng. 2014, 8(2): 179–187
DOI 10.1007/s11705-014-1431-0

RESEARCH ARTICLE

WO_3 nanomaterials synthesized via a sol-gel method and calcination for use as a CO gas sensor

Diah SUSANTI (✉)[1], A.A. Gede Pradnyana DIPUTRA[1], Lucky TANANTA[1], Hariyati PURWANINGSIH[1], George Endri KUSUMA[2], Chenhao WANG[3], Shaoju SHIH[3], Yingsheng HUANG[4]

1 Department of Materials and Metallurgical Engineering, Institut Teknologi Sepuluh Nopember (ITS), Surabaya 60111, Indonesia
2 Department of Mechanical Engineering, Surabaya State Shipbuilding Polytechnic, Institut Teknologi Sepuluh Nopember (ITS), Surabaya 60111, Indonesia
3 Department of Materials Science and Engineering, National Taiwan University of Science and Technology (NTUST), Taipei 10607, Taiwan, China
4 Department of Electronic Engineering, National Taiwan University of Science and Technology (NTUST), Taipei 10607, Taiwan, China

Abstract Carbon monoxide is a poisonous and hazardous gas and sensitive sensor devices are needed to prevent humans from being poisoned by this gas. A CO gas sensor has been prepared from WO_3 synthesized by a sol-gel method. The sensor chip was prepared by a spin-coating technique which deposited a thin film of WO_3 on an alumina substrate. The chip samples were then calcined at 300, 400, 500 or 600 °C for 1 h. The sensitivities of the different sensor chips for CO gas were determined by comparing the changes in electrical resistance in the absence and presence of 50 ppm of CO gas at 200 °C. The WO_3 calcined at 500 °C had the highest sensitivity. The sensitivity of this sensor was also measured at CO concentrations of 100 ppm and 200 ppm and at operating temperatures of 30 and 100 °C. Thermogravimetric analysis of the WO_3 calcined at 500 °C indicated that this sample had the highest gas adsorption capacity. This preliminary research has shown that WO_3 can serve as a CO gas sensor and that is should be further explored and developed.

Keywords WO_3 nanomaterial, sol-gel, calcinations, CO gas sensor, sensitivity

1 Introduction

Carbon monoxide is a hazardous gas which is colorless, odorless, tasteless, and difficult to dissolve in water. It can remain in the air for a long period of time, 1–5 years, due to the ability of the atmosphere to absorb it. In big cities the main source of CO gas is the incomplete combustion reaction of fossil fuels in motor vehicles and industrial plants. CO gas is also formed as a byproduct of human and animal metabolisms.

CO gas is very harmful to human health. People living and working close to heavy traffic and industrial factories are the most affected group. The effects of CO vary and depend on the overall health of an individual. CO poisoning worsens the condition of patients with heart and lung disorders, and it can cause premature delivery and death. CO hinders the transport of oxygen in the blood and can result in a lack of oxygen which causes the heart to work harder. The inhalation of large quantities of CO over a short time period can result in fainting and even death.

Sensitive sensors that can detect the presence of CO are very important. Tungsten trioxide is an n-type metal oxide semiconductor which has many applications including sensors for various substances such as NO_2 [1,2], CH_4, CO [3], NH_3 [4], methanol, *ter*-butanol, dimethyl methylphosphonate (DMPP), *iso*-propanol, hexanol [5], and acetone [6]. WO_3 has also been used in electrochromic devices (smart windows) [7–10], and in electrochemical capacitors [11]. The optimal performance of the WO_3 nanomaterials in these devices depends on the electrical conductivity and surface adsorption properties of the material which are closely related to the structure, morphology and size of the material [12,13].

Many methods have been used to synthesize WO_3 nanomaterials and these methods have resulted in different structures, morphologies and properties. Some of the methods include sol-gel processes [1,7–9], hydrothermal processes [2,4,14], spray pyrolysis [3], cathodic electrodeposition [10], solid-fed flame synthesis [13], laser ablation [15], solvothermal synthesis [16], chemical vapor deposition [17], reactive sputtering [18], liquid

Received July 24, 2013; accepted January 22, 2014

E-mail: santiche@mat-eng.its.ac.id

phase deposition [19], and a colloidal gas aphrons method [20]. Among these methods, the sol-gel process is a relatively cheap, simple and easy procedure since it does not need strict control of the temperature and pressure. In addition, it has been successfully applied in industries for the mass production of thin and thick films with controllable sizes, shapes, and homogeneities.

In a sol-gel process, an "aqueoussol" is transformed into a "solid" gel. However, since a gel is still wet and amorphous even after drying, thermal treatment at a higher temperature is usually carried out. The thermal treatment is intended to eliminate volatile matter, break intermolecular bonds in the substances, and assist in thermal decomposition, phase transitions, and structure modifications including crystallization [21]. High temperature calcination is commonly employed as the thermal treatment process. Wang et al. used calcination at different temperatures to modify the crystalline structures of WO_3 nanomaterials for NO_2 gas sensor applications [1]. The sensitivities toward NO_2 gas strongly depended on the structure of the WO_3 nanomaterials which resulted from different calcination temperatures.

Although many papers have reported the application of WO_3 in various gas sensors, the application of WO_3 as a CO gas sensor has rarely been reported. SnO_2, TiO_2 and Ga_2O_3 are the most common semiconductor materials used in CO gas sensors [22]. Therefore in this research WO_3 nanomaterials were synthesized by a sol-gel method followed by calcination and the WO_3 was then applied as a CO gas sensor. X-ray diffraction (XRD), scanning electron microscopy (SEM), high resolution transmission electron microscopy (HRTEM), energy dispersive X-ray (EDX) spectroscopy, Raman spectroscopy, Brunauer Emmet Teller (BET) surface area analysis, differential thermal analysis (DTA) and thermo gravimetry analysis (TGA) were used to characterize and compare the structures and morphologies of the resulting nanomaterials. The sensitivity of the sensors for CO gas was measured by determining the resistance changes of the sensor chip before and after CO gas exposure. This research proves the ability of WO_3 to act as a CO gas sensor.

2 Experimental

The sol-gel process to produce the tungsten trioxide nanomaterial has been previously reported by our group [23]. First 7 g of WCl_6 (Acros Organics) was mixed with 100 mL of C_2H_5OH to produce the tungsten alkoxide precursor, $W(OC_2H_5)_6$. Next 10 mL of 0.5 M NH_4OH solution was added to the precursor as a catalyst and the solution was stirred for 24 h under ice cooling while the hydrolysis and condensation processes occurred. The chloride ions were then removed by washing the precipitate with de-ionized-water and centrifuging until no AgCl precipitate appeared when 0.1 M $AgNO_3$ solution was added. The washed precipitate was then peptized using ammonia hydroxide. Finally 50 μL of surfactant (Triton X-100) was added to the solution and the WO_3 gel was formed.

The gel was spin-coated onto a polished surface of alumina (Al_2O_3) substrate (20 mm× 20 mm× 2 mm) at a rate of 500 rpm for 30 s and then at 2000 rpm for 90 s. The alumina substrate was cleaned with de-ionized water and acetone prior to use. The WO_3 gels coated on top of the alumina substrates were then calcined at 300, 400, 500 or 600 °C for 1 h. The samples were slowly cooled to room temperature inside the furnace to allow the particles to from well-ordered arrays and crystalline solids.

Scanning electron microscopy (SEM, FEI S-50 with a working voltage of 20 kV) and high resolution transmission electron microscopy (HRTEM, FEI Tecnai G^2 with a working voltage of 200 kV equipped with an energy dispersive X-ray spectrometer) were used to observe the morphologies and chemical compositions of the materials. X-ray diffraction (XRD Philips X-Pert XMS) using a Cu Kα X-ray source with a wavelength of 1.54056 Å and a Ni-filter was used to observe the structures and crystalline sizes of the materials. The XRD measurements were carried out from 2θ = 20° to 90° with a scan rate of 0.02° s^{-1}. Thermo gravimetric analysis and differential thermal analysis (TGA/DTA, Mettler Toledo) were used to measure the moisture content and to inspect the structural changes that occurred when the temperature was increased from room temperature to 600 °C. BET (Quantachrome Autosorb iQ) analysis was used to measure the active surface area and material pore sizes in the WO_3. Fourier transform infrared spectroscopy (Shimadzu FTIR 8400S) from 400 to 4000 cm^{-1} and Raman spectroscopy (Renishaw) were used to identify the functional groups in the WO_3 samples. HRTEM, EDX, TGA/DTA, BET, FTIR, and Raman measurements of WO_3 powder were also performed.

The sensor chips were assembled as follows. First, both ends of the WO_3-spin-coated alumina wafer were sputtered with palladium (2 mm in width) for 3 min to form current collectors. The back side of the alumina substrate was also sputtered with Pd in a 1-mm-wide zigzag-line shape to form a heater. To measure the sensitivity for CO gas, the sensor chip was placed in a chamber. Both the current collectors were connected to Cu wires which extended out of the chamber and were connected to the electrochemical measurement device (Solartron Instrument). Both ends of the Pd heater were also connected to Cu wires which were connected to the thermocontroller device outside of the chamber. Figure 1 shows the schematic diagram of the sensor chip arrangement.

To measure the sensitivity, the chip temperature was set at 200 °C and the resistance of the chip in air (denoted as R_o) was measured by applying a constant potential difference of 3 V using the potentiostat mode of the

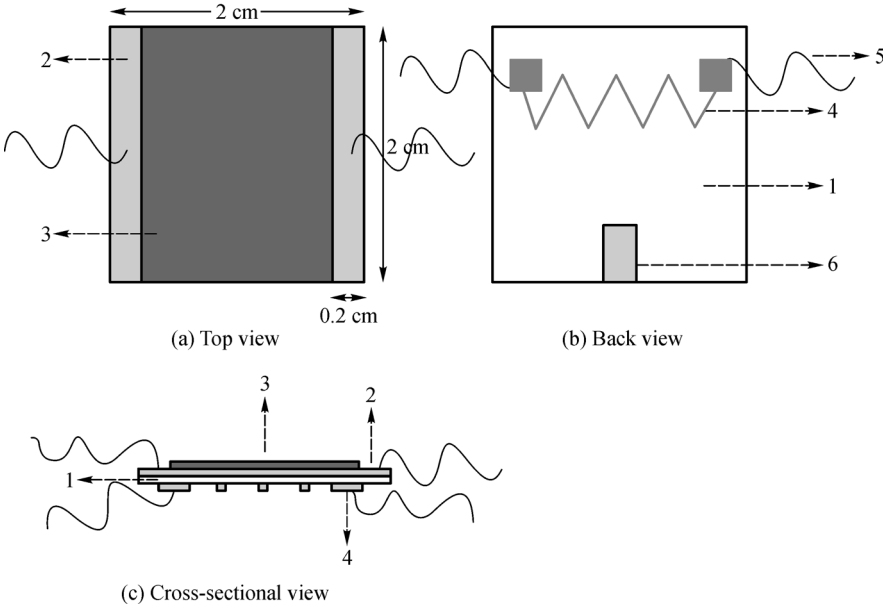

Fig. 1 Schematic diagram of the sensor chip arrangement. 1 Alumina substrate, 2 palladium electrode, 3 WO_3 film, 4 palladium heating element, 5 connecting wires, 6 small ceramic tube for thermocouple connection

Solartron instrument. CO gas was then introduced into the chamber so that the concentration of CO gas was 50 ppm and the resistance of the chip was then recorded. This resistance is denoted as R_g. This measurement was applied to the four samples that were calcinated at 300, 400, 500, and 600 °C. The sensitivity (S) was defined as the ratio of the absolute difference between R_g and R_o to R_o, which is mathematically expressed as Eq. (1):

$$S = \frac{|R_g - R_o|}{R_o}. \quad (1)$$

These measurements were conducted to find the sample with the highest sensitivity for CO gas. After this sample was identified, further measurements were performed on this sample. The CO sensitivity changes at other CO concentrations (100 ppm and 200 ppm) at 200 °C and at other operation temperatures (30 °C and 100 °C) at 200 ppm CO were measured.

3 Results and discussion

Figure 2 depicts the secondary electron SEM images of the WO_3 films coated on top of the alumina wafers after they were calcined at 300, 400, 500 or 600 °C. The WO_3 particles are grainy thin transparent slabs. These shapes are similar to those reported previously [23]. The size of particles increased with increasing calcination temperature. For example, the particles calcinated at 300 °C were 161–322 nm whereas those calcinated at 600 °C were 407–1142 nm. At higher temperature more energy is available for the particles to grow larger. This result is similar to the results of Wang et al. [1] who also reported that particle sizes increased with calcination temperature.

The XRD patterns of the WO_3 materials are shown in Fig. 3. As the calcination temperature increased, the XRD peaks became sharper with higher intensities. Hence, the crystallinity was enhanced with increasing calcination temperature. The XRD patterns of the samples calcined at 300 °C and 400 °C have broader and less intense peaks which is an indication of semi-crystalline materials.

Based on the XRD analysis, two different structures of WO_3 were identified. The XRD pattern of the sample calcined at 300 °C is consistent with a WO_3 hexagonal structure (PDF No 85-2459) where the three dominant crystalline plane orientations are (002), (112) and (321) at 2θ = 23.197°, 33.832°, and 65.2° respectively. For the samples calcined at 400 °C and higher, the XRD patterns show a WO_3 monoclinic structure (PDF No 83-0950) with three dominant planes of (002), (200), and (020) at 2θ = 23.117°, 23.583°, and 24.367° respectively. The most intense peak at 2θ = 41.7° is due to the alumina substrate, the (006) plane (PDF No 41-1230). The polymorphism of the WO_3 crystalline structure is a function of the calcination temperature. The hexagonal phase is meta-stable, whereas the stable phase at room temperature is monoclinic or orthorhombic [24].

The crystallite size (D, in nm) of a material can be calculated using the Scherrer formula:

$$D = \frac{0.9\lambda}{B\cos\ \theta}, \quad (2)$$

where λ is the wavelength of X-ray radiation (nm), B is the

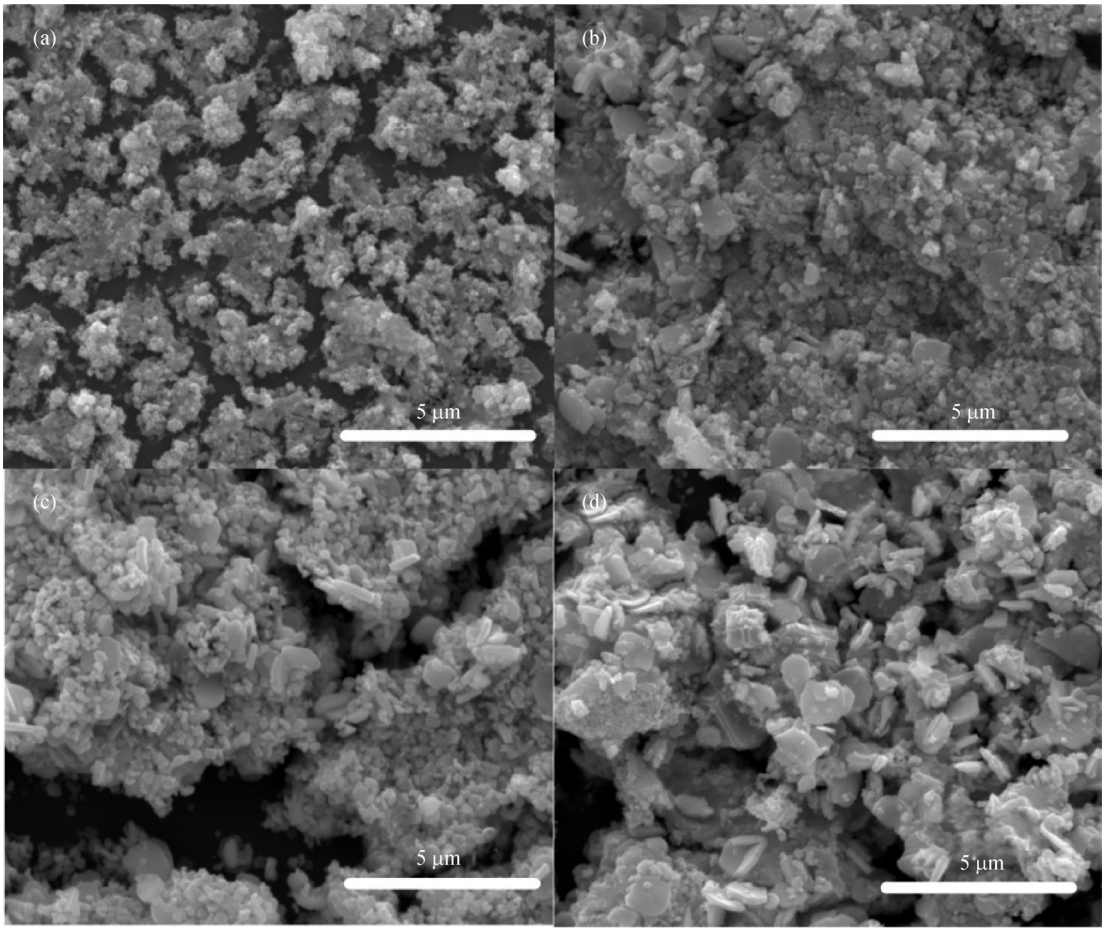

Fig. 2 Secondary electron SEM images of WO_3 coated on top of alumina wafers after calcination at (a) 300, (b) 400, (c) 500, and (d) 600 °C for 1 h

full width at half maximum (FWHM, radian), and θ is Bragg's angle (degree) [25]. The crystalline sizes of WO_3 were calculated using Eq. (2) and are shown in Table 1. Obviously, the crystalline size increases with increasing calcination temperature. Also, Table 1 lists the active surface areas of WO_3 powder calcined at 300, 400, 500 and 600 °C. The active surface area decreased as calcination temperature increased. Bigger particles always have smaller active surface areas.

To observe the morphology of the WO_3 materials in more detail, HRTEM analysis was performed on the sample calcined at 600 °C and the results are displayed in Fig. 4. Figure 4(a) shows a cluster of the WO_3 material which is 100–250 nm in width and 400–600 nm in length and consists of about 30 particles. Figure 4(b) shows the higher magnification of the square region in (a). Magnifications of the square regions (1) and (2) in Fig. 4(b) are shown in Fig. 4(c) and 4(d) respectively. The lattice spacings are 0.35 nm and 0.37 nm which correspond to the (020) and (200) planes respectively. These planes are also identified in the XRD analysis shown in Fig. 3.

The chemical analysis of the WO_3 material was determined using EDX spectroscopy and the results are shown in Fig. 5. The synthesized nanomaterial only contained W and O and had no impurities. The Cu signal is from the Cu film grid and the Fe and Co signals are from the TEM holder.

Figure 6 shows the Raman spectra of WO_3 powder calcined at 300, 400, 500 and 600 °C. Generally the Raman peaks were enhanced as the calcination temperature increased. These results are in line with the XRD results showing that the crystallinity was enhanced with increasing calcination temperature. The Raman peaks above 1200 cm^{-1} are attributed to the water content and they disappeared when the calcination temperature was above 400 °C. Hence, the samples calcined above 400 °C were crystalline, whereas those calcined at 400 °C and below were semi-crystalline materials.

The peaks at about 715 and 807 cm^{-1} are due to the O–W–O stretching modes (ν (O–W–O)), whereas those at about 273 and 327 cm^{-1} are from the O–W–O bending modes (δ (O–W–O)) of monoclinic WO_3. The hexagonal phase of WO_3 is indicated by the Raman peaks at about 645, 690, and 817 cm^{-1} which are due to the O–W–O

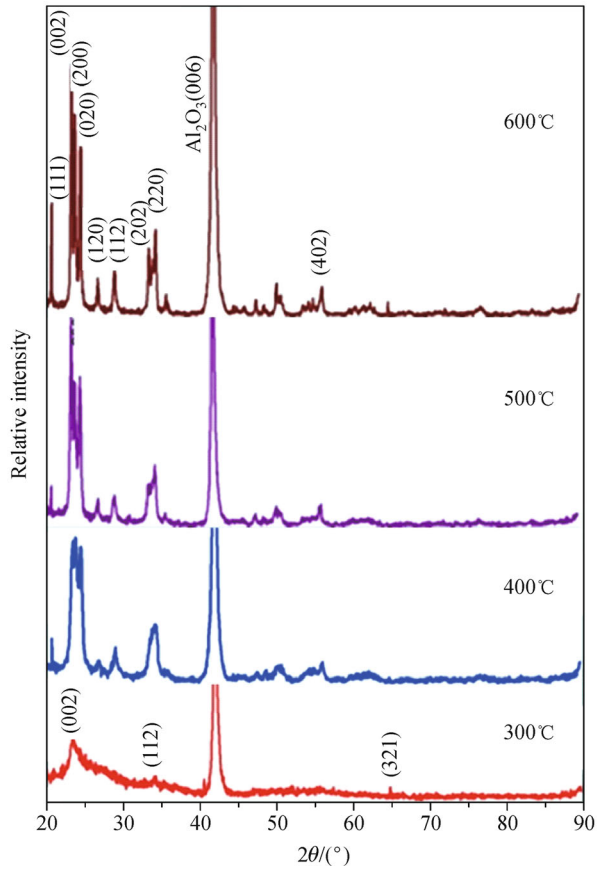

Fig. 3 X-ray diffraction patterns of WO_3 material after calcination at 300, 400, 500, and 600 °C for 1 h

stretching modes (ν (O–W–O)) and those at about 253 and 320 cm^{-1} which are due to the W–O–W stretching modes (ν (W–O–W)) [26]. Therefore, the samples calcined at 400 °C and above have monoclinic structures, whereas the sample calcined at 300 °C has a hexagonal structure.

Figure 7 shows the TGA/DTA results of the WO_3 powder. A TGA/DTA analysis was performed on a WO_3 gel in order to explore the weight and heat changes of the material during heating (Fig. 7(a)). The weight of the material decreased sharply, as much as 70%, below 90 °C which is the result of the removal of large amounts of physically bonded water and other volatile materials. This process is indicated by the first endothermic peak at 90 °C. There are no significant weight changes observed from 90 to 170 °C. The second endothermic peak at 230 °C is indicative of the vaporization of a small amount (~5%) of chemically bonded water. Above 230 °C the material weight loss is only 0.8%, which is probably due to the removal of oxygen [4].

The sample calcined at 300 °C (Fig. 7(b) lost more weight than any of the other calcined samples. It lost 2.5% of its weight below 90 °C (from the loss of water and other volatiles), 1.7% from 90 to 230 °C and 2.8% from 230 to 600 °C. The total loss was 7%, whereas the sample calcined at 400 °C lost only 0.64% upon heating to 343 °C. When heated to above 343 °C, the sample regained 0.12% due to the adsorption of gasses. Hence, the semi-crystalline structures of these two samples that was indicated by the XRD and Raman analyses is due to the presence of some water and other volatile matter.

The TGA of the samples calcined at 500 and 600 °C are

Table 1 Crystallite sizes and active surface areas of WO_3 powder calcinated at different temperatures

Calcination temperature /°C	300	400	500	600
Crystallite size /nm	6.4	10.9	21.8	39.3
BET surface area /($m^2 \cdot g^{-1}$)	83.94	15	11.2	4.51

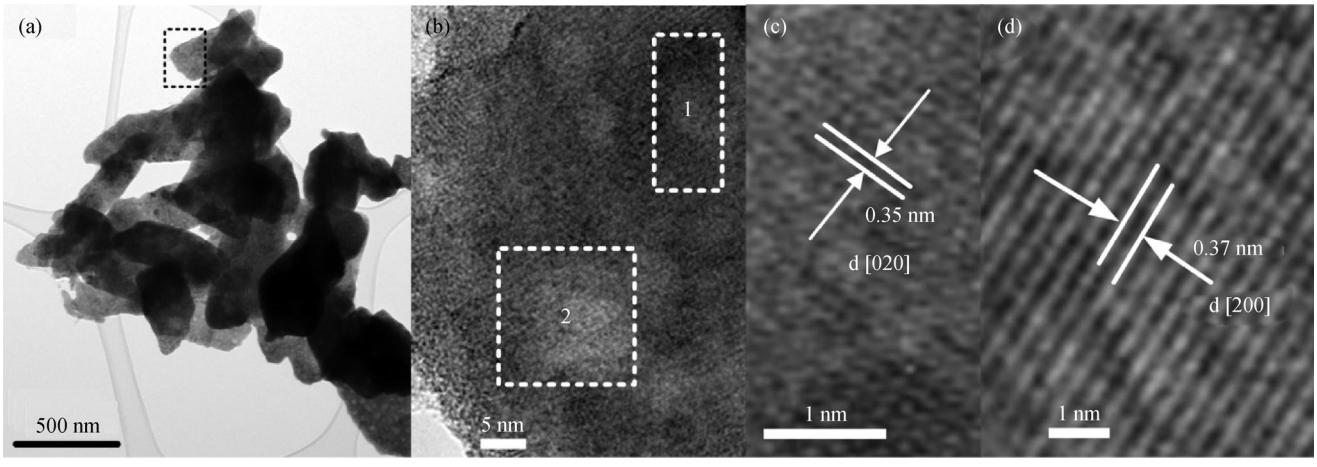

Fig. 4 Bright-field TEM images of the WO_3 material calcined at 600 °C. (a) A WO_3 cluster, (b) higher magnification of the square region in (a), (c) and (d) magnified images of the square regions in (b), 1 and 2 respectively

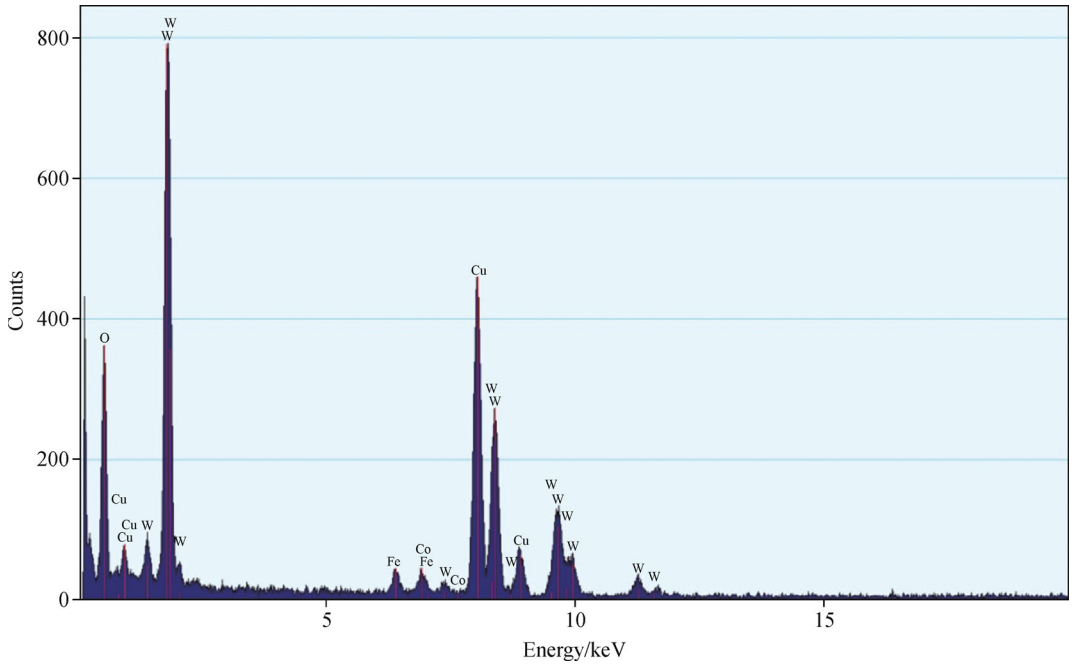

Fig. 5 EDX spectra of WO_3 taken from the square region in Fig. 4(a)

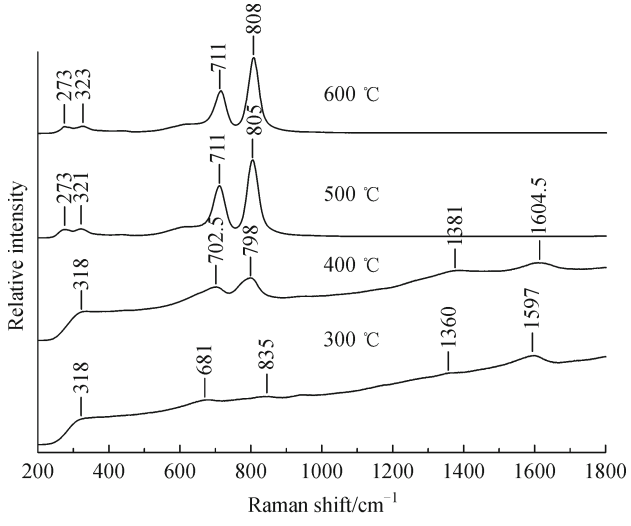

Fig. 6 Raman spectra of WO_3 powder calcined at 300, 400, 500, and 600 °C

shown in Fig. 7(c). Both these samples gained weight as they were heated. The weight of the sample calcined at 500 °C increases 4.29% on heating from room temperature to 600 °C, whereas the weight of the sample calcined at 600 °C decreases 0.25% below 60 °C and then increases 2% when heated above 60 °C. The increase in sample weights is probably caused by gas adsorption since the DTA result in Fig. 7(a) does not show any phase transformations peaks but only shows the vaporization processes. Hence, the WO_3 sample calcined at 500 °C has the best gas adsorption ability and would presumably be the most suitable for use as a gas sensor. Wang et al. reported that WO_3 calcined at 550 °C showed the best sensitivity for NO_2 gas adsorption [1].

Figure 8(a) depicts the sensitivity for CO by the sensors prepared by different calcination temperatures. The sensor calcined at 500 °C had the highest sensitivity for CO gas. This result is supported by the TGA data in Fig. 7(c) which shows that the sample calcinated at 500 °C had the best ability for gas adsorption.

It is important to understand the reasons that the sample calcinated at 500 °C had the best CO sensitivity. The structure of a material drastically affects the properties of that material including its sensitivity to certain gases.

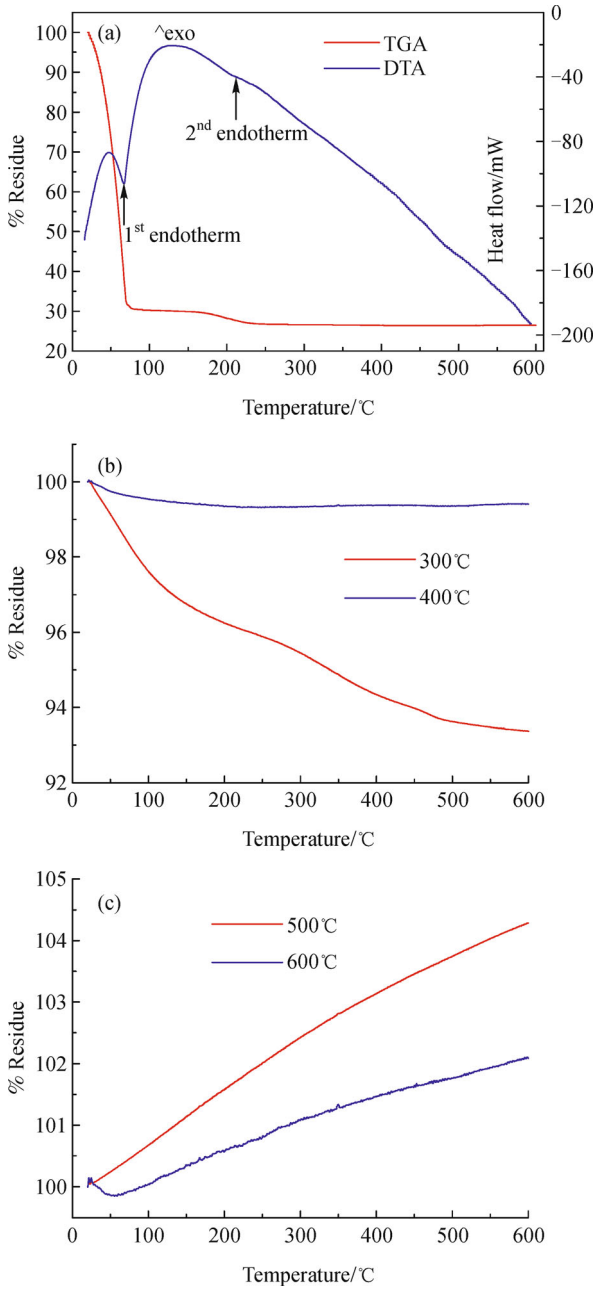

Fig. 7 (a) TGA/DTA of WO_3 gel without thermal treatment, (b) TGA of WO_3 powder treated at 300 and 400 °C, (c) TGA of WO_3 powder treated at 500 °C and 600 °C

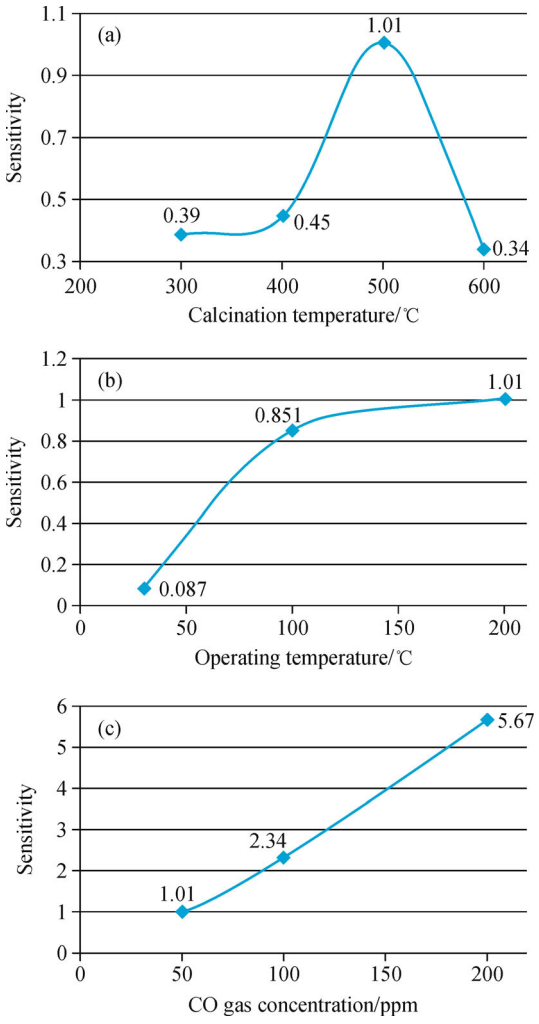

Fig. 8 (a) Sensitivity of WO_3-based chip sensor calcined at 300, 400, 500 and 600 °C, measured at 200 °C and 50 ppm CO; (b) Sensitivity of sensor calcined at 500 °C measured at different operating temperatures: 30, 100 and 200 °C at 50 ppm CO; (c) Sensitivity of sensor calcined at 500 °C measured at different CO gas concentrations: 50, 100 °C and 200 ppm at 200 °C

Tamaki et al. [27] reported that the grain size strongly influences the sensitivity of WO_3 to nitrogen oxides. The sensitivity of the sensor increased as the grain size decreased. Hidayat et al. [13] reported that the adsorption performance of tungsten oxide for methylene blue depended on the particle size. The interactions between the surface atoms of tungsten oxide and the methylene blue molecules increased as the tungsten oxide particle sizes decreased. However in this work, the sample calcined at 500 °C did not have the smallest particles and crystallite sizes. Nor did it have the highest active surface area. These all belonged to the sample calcined at 300 °C (Fig. 2 and Table 1) which was not the most sensitive sample for CO gas.

The sensing properties of semiconductor materials depend on the structural defects (non-stoichiometric structures) and the free electrons that come from oxygen vacancies. There are more oxygen vacancies on WO_3 surfaces calcined at higher temperatures [1]. The material's crystallinity also plays a role in determining its sensing properties [4]. The sample calcined at 600 °C should have the highest number of oxygen vacancies and the best crystallinity since it was calcined at the highest temperature. However, it had the lowest sensitivity for CO gas. Therefore there must be some interdependencies among

the various aspects, such as particle size, crystallite size, active surface area, oxygen vacancies, and crystallinity, which affect the sensitivity for CO.

The CO gas detection process can be written as:

$$\frac{1}{2}O_{2(g)} + e^- \rightarrow O^-_{ads} \quad (3)$$

$$CO_{(g)} + O^-_{ads} \rightarrow CO_{2(g)} + e^- . \quad (4)$$

The first reaction describes the adsorption of oxygen from the air onto the surface of WO_3 as a sensor material and the second reaction describes the surface reaction between CO gas and the oxygen ion. The chemisorbed oxygen molecules attract electrons from the conduction band of WO_3 and are reduced to different ionic forms such as O^-, O_2^- and O^{2-} which results in a reduction of the electrical conductivity of the material. When this material is then exposed to reductive gases, such as CO, the chemisorbed oxygen will react with the gases and release the electrons back to the conduction band, leading to an increase in the material electrical conductivity. In a good gas sensor, the changes in material conductivity must be great and proportional to the gas concentration [28].

The density of electrons at the tungsten oxide surface increases with the operating temperature [1]. The more electrons that are attracted to the material surface, the lower the material's conductivity will be. Therefore, the sensitivity of WO_3 toward CO gas increased with operating temperature as shown in Fig. 8(b). Moreover, when there is more CO gas near the surface of the material sensor, more oxygen ions react with the CO gas and more electrons are released back in the conduction band of the material. As a result, the conductivity of the material decreases and the sensitivity of the sensor material increases. Figure 8(c) shows that as expected the sensitivity of the WO_3 sensor increased as the CO gas concentration increased.

4 Conclusions

WO_3 nanomaterials have been synthesized by a sol-gel method followed by calcination at 300, 400, 500 or 600 °C for 1 h. The nanomaterials were then applied as CO gas sensors. The sensitivity of the material toward CO gas depended on the calcination temperature which affected the material's structure. WO_3 calcined at 500 °C had the best sensitivity for CO gas due to its good ability to adsorb gas. The sensitivity of the sensor also depended on the sensor operating temperature and the CO gas concentration. Sensitivity increased as both operating temperature and CO gas concentration increased. These results show that WO_3 can serve as a CO gas sensor and it should be further explored and developed.

Acknowledgements The authors gratefully acknowledge the financial support and facilities provided by the Ministry of Research and Technology Republic of Indonesia through Applied Research Incentive 2012 No 0161.12/IT2.7/PM/2012 and Institut Teknologi Sepuluh Nopember (ITS)-Surabaya Indonesia through International Collaboration Research Grant 2011 No 0750.042/I2.7/PM/2011.

References

1. Wang S H, Chou T C, Liu C C. Nano-crystalline tungsten oxide NO_2 sensor. Sensors and Actuators. B, Chemical, 2003, 94(3): 343–351
2. Liu Z, Miyauchi M, Yamazaki T, Zhen Y. Facile synthesis and NO_2 gas sensing of tungsten oxide nanorods assembled microspheres. Sensors and Actuators. B, Chemical, 2009, 140(2): 514–519
3. Boulova M, Gaskov A, Lucazeau G. Tungsten oxide reactivity versus CH_4, CO and NO_2 molecules studied by Raman spectroscopy. Sensors and Actuators. B, Chemical, 2001, 81(1): 99–106
4. Yan A, Xie C, Zeng D, Cai S, Hu M. Synthesis, formation mechanism and sensing properties of WO_3 hydrate nanowire netted-spheres. Materials Research Bulletin, 2010, 45(10): 1541–1547
5. Kanan S M, Tripp C P. Synthesis, FTIR studies and sensor properties of WO_3 powders. Current Opinion in Solid State and Materials Science, 2007, 11(1–2): 19–27
6. Su X, Li Y, Jian J, Wang J. In situ etching WO_3 nanoplates: Hydrothermal synthesis, photoluminescence and gas sensor properties. Materials Research Bulletin, 2010, 45(12): 1960–1963
7. Deepa M, Singh P, Sharma S N, Agnihotry S A. Effect of humidity on structure and electrochromic properties of sol-gel-derived tungsten oxide films. Solar Energy Materials and Solar Cells, 2006, 90(16): 2665–2682
8. Ozkan E, Lee S H, Liu P, Tracy C E, Tepehan F Z, Pitts J R, Deb S K. Electrochromic and optical properties of mesoporous tungsten oxide films. Solid State Ionics, 2002, 149(1–2): 139–146
9. Pyper O, Schollhorn R, Donkers J J T M, Krings L H M. Nanocrystalline structure of WO_3 thin Films prepared by the sol-gel technique. Materials Research Bulletin, 1998, 33(7): 1095–1101
10. Su L, Lu Z. All solid-state smart window of electrodeposited WO_3 and TiO_2 particulate film with PTREFG gel electrolyte. Journal of Physics and Chemistry of Solids, 1998, 59(8): 1175–1180
11. Chang K H, Hu C C, Huang C M, Liu Y L, Chang C I. Microwave-assisted hydrothermal synthesis of crystalline WO_3-$WO_3 \cdot 0.5H_2O$ mixtures for pseudocapacitors of the asymmetric type. Journal of Power Sources, 2011, 196(4): 2387–2392
12. Gillet M, Masek K, Gillet E. Structure of tungsten oxide nanoclusters. Surface Science, 2004, 566–568: 383–389
13. Hidayat D, Purwanto A, Wang W N, Okuyama K. Preparation of size-controlled tungsten oxide nanoparticles and evaluation of their adsorption performance. Materials Research Bulletin, 2010, 45(2): 165–173
14. Ha J H, Muralidharan P, Kim D K. Hydrothermal synthesis and characterization of self-assembled h-WO_3 nanowires/nanorods using EDTA salts. Journal of Alloys and Compounds, 2009, 475

(1–2): 446–451
15. Ramana C V, Utsunomiya S, Ewing R C, Julien C M, Becker U. Structural stability and phase transitions in WO_3 thin films. Journal of Physical Chemistry B, 2006, 110(21): 10430–10435
16. Houx N L, Pourroy G, Camerel F, Comet M, Spitzer D. WO_3 nanoparticles in the 5–30 nm range by solvothermal synthesis under microwave or resistive heating. Journal of Physical Chemistry B, 2010, 114: 155–161
17. Yous B, Robin S, Donnadieu A. Chemical vapor deposition of tungsten oxides: A comparative study by XPS, XRD and RHEED. Materials Research Bulletin, 1984, 19: 1349–1354
18. Pyun S I, Kim D J, Bae J S. Hydrogen transport through r.f. magnetron sputtered amorphous and crystalline WO_3 films. Journal of Alloys and Compounds, 1996, 244(1–2): 16–22
19. Deki S, Beleke A B, Kotani Y, Mizuhata M. Synthesis of tungsten oxide thin film by liquid phase deposition. Materials Chemistry and Physics, 2010, 123(2–3): 614–619
20. Abdullah S F, Radiman S, Hamid M A A, Ibrahim N B. Effect of calcinations temperature on the surface morphology and crystallinity of tungsten (VI) oxide nanorods prepared using colloidal gas aphrons method. Colloids and Surfaces A, 2006, 280: 88–94
21. Brinker C J, Scherer G W. Sol-Gel Science: The Physics and Chemistry of Sol-Gel Processing. San Diego, USA: Academic Press. Inc., 1990, 2–6
22. Ho G W. Gas sensor with nanostructured oxide semiconductor materials. Science of Advanced Materials, 2011, 3(2): 150–168
23. Susanti D, Nugroho S H, Nisfu H, Nugroho E P, Purwaningsih H, Kusuma G E, Shih S J. Comparative analysis of WO_3 nanomaterial synthesized using a sol-gel method followed by calcination and hydrothermal treatments. Frontiers of Chemical Science and Engineering, 2012, 6(4): 371–380
24. Cullity B D, Stock S R. Elements of X-Ray Diffraction. 3rd ed. New Jersey, USA: Prentice Hall, 2001, 170–172
25. Szilágyi I M, Madarász J, Pokol G, Király P, Tárkányi G, Saukko S, Mizsei J, Tòth A L, Szabò A, Varga-Josepovits K. Stability and controlled composition of hexagonal WO_3. Chemistry of Materials, 2008, 20(12): 4116–4125
26. Daniel M F, Desbat B, Lassegues J C, Gerard B, Figlarz M. Infrared and Raman study of WO_3 tungsten trioxide and $WO_3 \cdot xH_2O$ tungsten trioxide hydrate. Journal of Solid State Chemistry, 1987, 67 (2): 235–247
27. Tamaki J, Zhang Z, Fujimori K, Akiyama M, Harada T, Miura N, Yamazoe N. Grain-size effects in tungsten oxide-based sensor for nitrogen oxides. Journal of the Electrochemical Society, 1994, 141 (8): 2207–2210
28. Kocemba I, Rynkowski J. The influence of catalytic activity on the response of Pt/SnO_2 gas sensors to carbon monoxide and hydrogen. Sensors and Actuators. B, Chemical, 2011, 155(2): 659–666